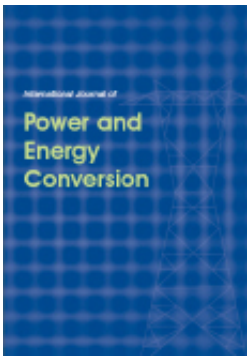

International Journal of Power and Energy Conversion

ISSN online: 1757-1162 - ISSN print: 1757-1154
https://www.inderscience.com/ijpec

Architecture and research of photovoltaic hybrid microgrid control system combined with renewable energy

Guoku Wang

DOI: 10.1504/IJPEC.2024.10066183

Article History:

Received:	10 January 2024
Last revised:	06 June 2024
Accepted:	06 June 2024
Published online:	16 October 2024

Architecture and research of photovoltaic hybrid microgrid control system combined with renewable energy

Guoku Wang

Faculty of Petroleum Engineering,
Harbin Institute of Petroleum,
Harbin, 150028, China
Email: wang830324@126.com

Abstract: The issue of energy supply has become an important social problem, therefore, a photovoltaic hybrid power grid control system is proposed by combining renewable energy to improve the stability of microgrid systems. Based on the operating principles of direct drive wind power systems and photovoltaic power generation systems, a DC voltage source control strategy for wind and photovoltaic hybrid microgrids is proposed, and its effectiveness is verified through experiments. In the dynamic response of the hybrid microgrid during sudden changes in wind speed, the wind speed changes after t = 6s, and the active power of the photovoltaic power generation system decreases from 6,200 W to 5,500 W. Then, the important participating factors of the microgrid system were analysed, and as the trajectory of characteristic value movement changed, the DC voltage parameters of the photovoltaic power generation system were optimised to 2e-3, verifying the effectiveness and practicality of the proposed control system.

Keywords: renewable energy; hybrid microgrid; system; direct drive wind power; photovoltaic power generation.

Reference to this paper should be made as follows: Wang, G. (2024) 'Architecture and research of photovoltaic hybrid microgrid control system combined with renewable energy', *Int. J. Power and Energy Conversion*, Vol. 15, No. 5, pp.1–19.

Biographical notes: Guoku Wang is an Associate Professor in Master of Engineering and graduated from the Northeast Petroleum University in 2012 majoring in Engineering Thermophysics. At present, he serves as the Head of the Department of New Energy Science and Engineering in Harbin Petroleum Institute, mainly engaged in the research on the efficient utilisation of solar energy and the operation control of energy storage. He often visits Yunnan Normal University, Northeast Dianli University, Shandong Petrochemical University and other universities for research, and has published more than ten high-level academic papers such as Peking University Core. He published an international monograph entitled *Correlation between Performance of Foam Oil Displacement System and Solar Energy*.

1 Introduction

As the boost of global energy demand and the urgent need for environmentally friendly energy, renewable energy has gradually become a hot topic in the energy industry today. Photovoltaic power generation (PPG), as an efficient form of renewable energy, has been increasingly widely used (Rathore et al., 2021a; Badr et al., 2024; Rathore et al., 2023). Meanwhile, PPG systems face problems such as instability, intermittency, and randomness, which pose certain challenges to the safety, stability, and operational efficiency of the power grid (Kumar et al., 2023a; Mishra et al., 2024). To overcome these problems, hybrid microgrid technology has gradually received attention from researchers. A hybrid microgrid integrates multiple energy resources (including traditional and renewable energy) and energy storage (ES) devices to form an autonomous and interconnected power system. The hybrid microgrid system has a certain degree of autonomous operation and self-healing ability, which can continue to supply power in the event of faults or interruptions in the traditional power grid. However, to achieve effective integration of renewable energy and hybrid microgrid systems, an effective control system is essential for managing the power generation (PG) system and ES equipment. In view of this, this study proposes a control system architecture suitable for photovoltaic hybrid microgrids (PHM), and conducts in-depth research and experimental verification on it. The system proposed in the study can provide strong support for the development of PHM systems and promote the sustainable development of renewable energy.

The innovation of the research is as follows:

1 The control strategy proposed in the research facilitates the efficient collaboration between wind power and PPG systems by optimising the DC bus voltage.

2 The direct drive wind power system (DDWPS) under investigation employs an adaptive sag control strategy, which enables the output power to be automatically adjusted in accordance with the requirements of the power grid.

3 The integrated energy management system, which has been the subject of extensive research and development, is capable of optimising the charge and discharge strategy of the ES system in real time. The contributions of the research are as follows:

- This study proposes a hybrid microgrid control system architecture combining direct drive wind power and PPG. The system's stability and operational efficiency are enhanced through the implementation of an advanced DC voltage source (VS) control strategy.
- A dynamic maximum power point (MPP) tracking algorithm has been developed with the objective of ensuring that the PPG system can achieve maximum power output under different lighting conditions.
- An adaptive sagging control strategy has been devised to enable the (DDWPS to automatically adjust its output in accordance with fluctuations in the power grid demand and wind speed, thereby enhancing the system's adaptability and reliability.

The research of the constructed system contains four parts. The first is for summarising the study on renewable energy and microgrid systems by scholars around the world, and analyse their research results. The second is for constructing and analysing the proposed

system, and introduce the DC VS control strategy. The third part is for testing the system performance through experiments. The fourth part is to summarise the relevant outcomes, point out the demerits in the study, and propose future research directions.

2 Related works

Many scholars have studied microgrid systems. Lv et al. proposed a two-stage bidirectional power converter regulation implementation method in AC hybrid microgrids to address the issue of DC bus being easily damaged. The first stage of this method was composed of a virtual synchronous generator, which can respond to the inertia frequency in the simulated AC bus. The second level was equipped with built-in capacitors, which improve the DC bus voltage response. Finally, simulation experiments were conducted. The experiment showed that the method possesses practical significance (Lv et al., 2020). Scholars such as Azizpour et al. proposed an AC/DC fault current limiter for short-circuit fault currents. This current limiter had two AC and DC ports and a common current limiting resistor, which can limit the short-circuit current on the DC and AC sides in AC/DC hybrid PG systems. The experiment showed that the proposed limiter achieves the purpose of limiting faults by using only one current limiting resistor, and reduces the cost of ordinary current limiting resistors (Azizpour et al., 2023). Chang and other scholars proposed a distributed optimal sharing strategy in islanded AC/DC hybrid power grid (IHMG) to ensure the operation and efficiency of IHMG. This strategy did not require the use of any distributed communication lines and is on the ground of distributed power sources and integrated circuits for cost minimisation in IPS. The experiment showed that the proposed strategy could reach distributed generator power sharing with minimal cost and IPS with maximum efficiency, effectively improving the efficiency of IHMG (Chang et al., 2022). Tooryan et al. proposed a microgrid optimisation method for distributed energy management in hybrid microgrid systems. This method combined battery ES, thermal ES, photovoltaic arrays, etc. for minimising the operating cost of hybrid microgrids. Then, a comparative experiment was conducted on the proposed method, and the experiment proved the effectiveness of the proposed method (Tooryan et al., 2021).

Many scholars have conducted corresponding research on renewable energy. Nguyen Duc et al. proposed a demand response plan incentive payment pricing method in the application field of power systems, combined with new energy. This method was on the ground of the framework of maximising social welfare and ensures the interests of all participants. In addition, the study calculated the cost of renewable energy and explored the influence of renewable energy on pricing mechanisms. The experiment showed its feasibility (Nguyen Duc et al., 2022). Hofrichter and other scholars explored the optimal power ratio between electrolysis and renewable energy in hydrogen production. This study considered the proportion, scale effect, and cost between renewable energy and electrolytic electricity, and calculated the different proportions of real photovoltaic and wind power sites and electricity. The experiments showed that the optimal proportion of photovoltaic systems is between 14% and 73%, while the ideal proportion of wind energy is between 3.3% and 143% (Hofrichter et al., 2023). Ahmed and other scholars proposed a Gram Charlie method in large-scale integrated power systems. This method can be used to solve the optimal transmission switch for renewable energy and can converge quickly.

This study optimised OTS PG scheduling and network topology, which can be used for large-scale integration. The experiment shows that the method is effective in large-scale PG (Ahmed et al., 2022).

Table 1 Comparison between research methods and existing work

Method	*Major technology*	*Advantage*	*Shortcoming*	*Research improvements*
Lv et al. (2020)	Two-stage bidirectional power converter	Improved DC bus voltage response	May increase system complexity	DC voltage source control strategy is proposed to simplify control and enhance stability
Azizpour et al. (2023)	AC/DC fault current limiter	Limited fault current	Performance may be limited under high loads	Wider power fluctuation control
Chang et al. (2022)	Distributed optimal sharing strategy	No distributed communication lines required	Sensitive to communication failures	Power sharing is optimised by droop control strategy
Tooryan et al. (2022)	Microgrid optimisation	Minimisation of operating costs	Sensitive to initial parameters	Introduce dynamic adjustment mechanism to improve system adaptability
Nguyen Duc et al. (2022)	Demand response plan incentive payment pricing method	Ensure the interests of all participants	High implementation complexity	Simplify demand response with DC voltage control
Hofrichter et al. (2023)	Research on optimal power ratio between electrolysis and renewable energy	Optimised hydrogen production cost	Strong dependence on specific conditions	Improve system flexibility through DC voltage source control strategy
Ahmed et al. (2022)	Gram-Charlier method	Fast convergence for large-scale integration	The optimisation effect for specific types of systems is obvious	The application range and stability of the method are extended

Although many scholars have made significant research achievements on renewable energy and microgrid systems, traditional inverter control methods can have an impact on the stability of microgrids. A photovoltaic hybrid microgrid control system (PHMCS) combining renewable energy is proposed, which can improve the stability of the hybrid microgrid and has practicality and effectiveness. The comparison and improvement between the research method and the existing work are shown in Table 1.

3 Construction of a PHMCS combined with renewable energy

The construction of a PHMCS combining renewable energy is divided into two parts. One part is the analysis of control strategies for PHMs. The other part is the research on PHM systems.

3.1 Control strategy for PHM

To combine renewable energy to build a PHMCS, the PHMCS is divided into three parts: direct drive wind power, PPG, and ES. The structure of the photovoltaic micro electric control system is shown in Figure 1.

Figure 1 Structure diagram of PHMCS (see online version for colours)

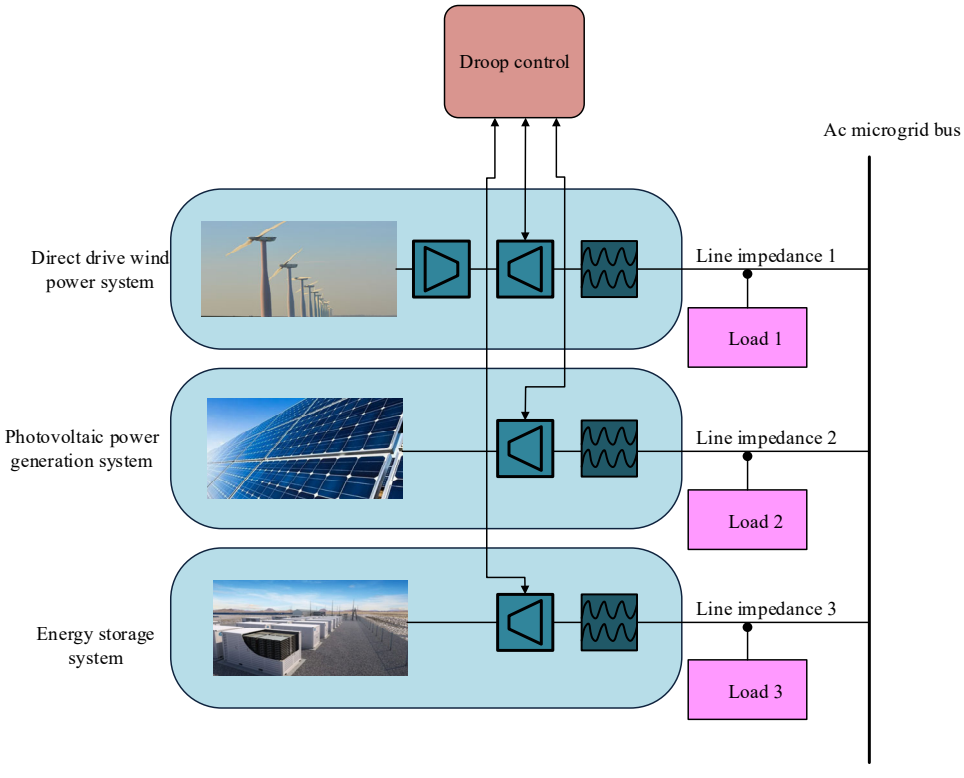

Figure 1 shows the PHMCS. In this system, to fully achieve the maximum efficiency of wind and solar energy, the maximum power of wind and photovoltaic power is controlled in the system. The traditional control method of power electronic converters requires the use of an external power grid to adjust the output power of the power source, which is highly dependent on the external power grid (Rathore, 2022; Gupta et al., 2022; Rathore et al., 2020). After the penetration rate of PG increases, this control method will cause serious power fluctuations in the microgrid control system. Therefore, traditional control methods for power electronic converters are not suitable for autonomous operation of microgrids. The autonomous operation of microgrids requires distributed generation units

to reasonably allocate load power (Pande et al., 2021; Kumar et al., 2023b; Rathore et al., 2021b). The control strategy of microgrids consisted of two methods. Microgrids that adopt master-slave control are highly dependent on the main control unit, usually undertaken by ES. However, when the main control unit experiences abnormalities, the microgrid system may experience fluctuations or even collapse. Therefore, peer-to-peer control strategy is used in PHMs, and the strategy used in microgrids under peer-to-peer control is droop control strategy. The basic formula for sag control strategy is expressed as formula (1).

$$\begin{cases} \omega = \omega_0 - m_p P \\ V = V_0 - n_q Q \end{cases} \tag{1}$$

In formula (1), ω_0 represents the frequency output by the power electronic converter under no-load conditions, and V_0 represents the voltage output by the power electronic converter under no-load conditions. m_p represents the active droop coefficient, n_q represents the reactive droop coefficient, and m_p and n_q also represent the slope of the droop curve. This is inversely proportional to the rated power. P serves as the active power (AP) output by the PG unit, and Q represents the reactive power (RP) output by the PG unit. n_q and m_p combine the inverter to allocate the system load reasonably, as shown in formula (2).

$$\begin{cases} m_{p1}P_1 = m_{p2}P_2 = m_{p3}P_3 = \ldots = m_{pn}P_n \\ n_{q1}Q_1 = n_{q2}Q_2 = n_{q3}Q_3 = \ldots = n_{qn}Q_n \end{cases} \tag{2}$$

In formula (2), m_{pn} represents the active droop coefficient of the distributed power source, n_{qn} represents its reactive droop coefficient, and P_n and Q_n serve as the output AP and RP. When wind PG becomes the main module in the autonomous operation system of microgrids, wind turbines (WT) and power electronic converters can help stabilise the voltage of the microgrid. The grid side converter must operate as a VS, controlling the voltage amplitude and frequency through adjusting reactive and AP. The control method of the VS is showed in Figure 2.

Figure 2 is a schematic diagram of the VS control strategy for a DDWPS. The basic idea of a DDWPS is to convert the wind energy captured by the WT into rotational mechanical energy. However, changes in wind energy can cause fluctuations in the rotational mechanical energy of the generator, leading to further fluctuations in output frequency and voltage. Therefore, it is necessary to use a machine side rectifier for rectification, and the unstable AC power is rectified into DC and transmitted to the DC bus. In a direct drive wind power VS system, the relationship between the wind energy captured by the WT and other power is shown in formula (3).

$$\begin{cases} P_g - P_{WT} = V_{dc} i_{dc} = V_{dc} C \dfrac{dV_{dc}}{dt} \\ P_{wind} = \dfrac{1}{2} \rho A C_p (\beta, \omega_s) v^3 \end{cases} \tag{3}$$

Figure 2 VS control strategy diagram of DDWPS (see online version for colours)

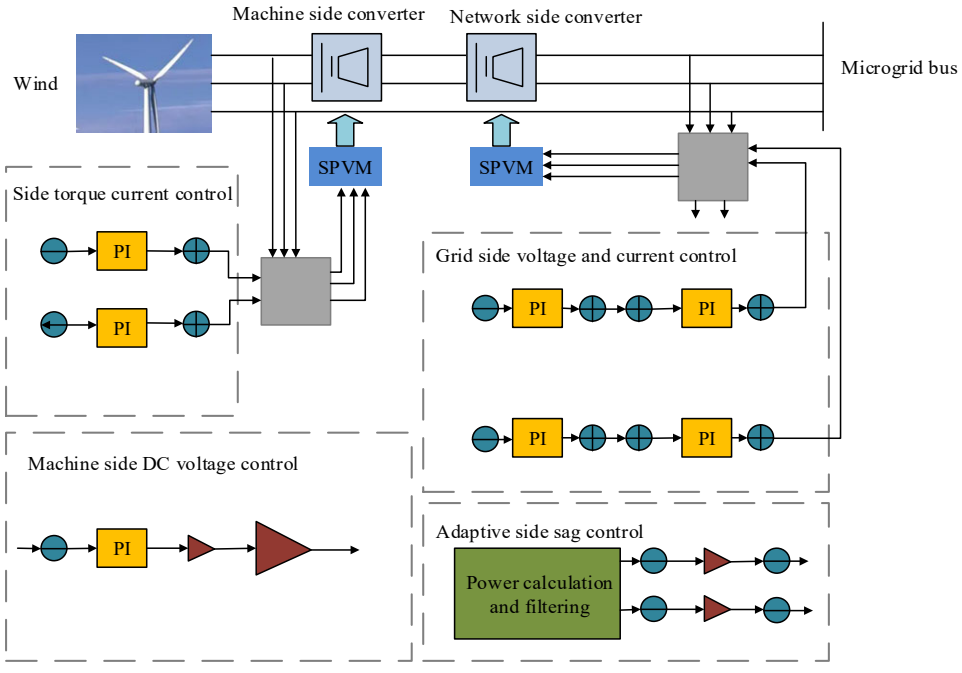

In formula (3), P_{wind} represents the wind energy captured by the WT, P_g represents the output power, and P_{WT} represents the output power of the grid side inverter. V_{dc} and i_{dc} represent the DC voltage and current of the intermediate capacitor, ω_s serves as the generator speed, and β serves as the pitch angle of the WT. It assumes that there is no loss in the power converter, and the power output of the generator is equal to the wind energy captured by the WT during stable operation. When the output power of the grid side inverter changes, the generator speed also changes, so that the generator output power matches F. The DDWPS utilises a dynamic droop control strategy to combine the maximum power of the direct drive generator with the power droop loop, achieving VS droop control. Adaptive sag control is a system that automatically adjusts the output power in response to changes in the frequency and voltage of the grid. MPP tracking is a method of dynamically adjusting the working state of the photovoltaic array according to real-time environmental data. The expression for the adaptive droop control strategy of a DDWPS is formula (4).

$$\begin{cases} \omega_{WT} = \omega_n^{WT} - m_P^{WT}\left(P_{WT} - P_{WT}^*\right) + K_{p\omega s}\left(\omega_s - \omega_s^{ref}\right) + K_{i\omega s}\int\left(\omega_s - \omega_s^{ref}\right)dt \\ V_{WT} = V_n^{WT} - n_Q^{WT}\left(Q_{WT} - Q_{WT}^*\right) \end{cases} \tag{4}$$

In formula (4), ω_n^{WT} and n_Q^{WT} represent the rated frequency and voltage, respectively, and ω_s^{ref} represents the speed corresponding to the MPP on the WT transmission power curve. P_{WT} and Q_{WT} respectively represent the actual AP and RP output of the grid side inverter. ω_{WT} represents the output angular frequency of the DDWPS, and V_{WT} represents the voltage amplitude of the DDWPS. P_{WT}^* and Q_{WT}^* represent the active and reactive

droop coefficients of the DDWPS, respectively. For ensuring the stability of the voltage and frequency of the autonomous microgrid under high utilisation of new energy, photovoltaic reverse transformers are selected as the VS. Therefore, the VS control strategy of the PPG system is showed in Figure 3.

Figure 3 PV VS control strategy framework (see online version for colours)

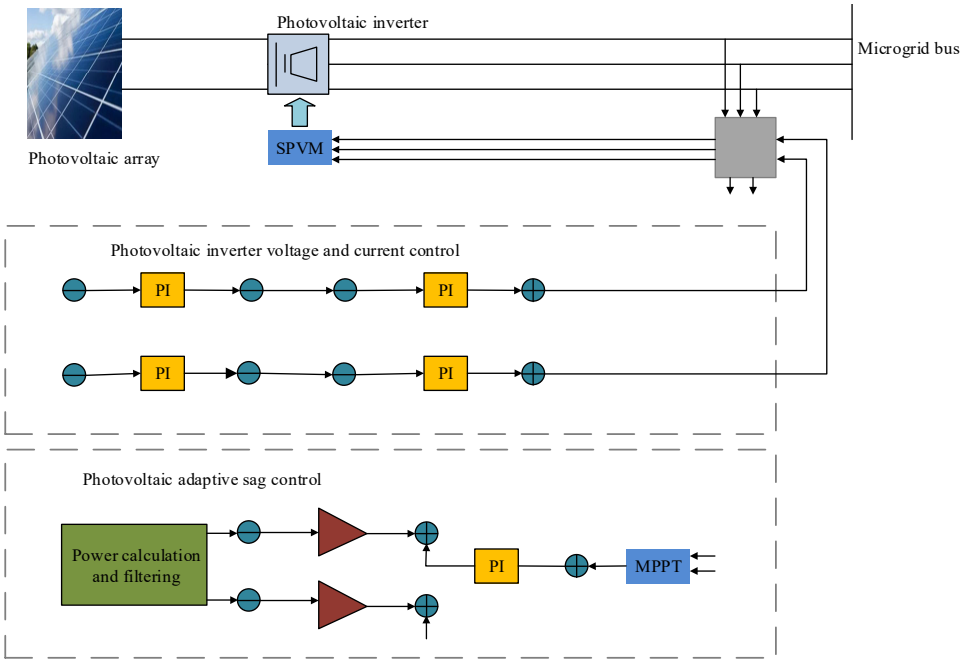

Figure 3 shows the framework of photovoltaic VS control strategy. The core components of the photovoltaic VS system are power droop control and DC voltage control (Pandey et al., 2022). In inverter voltage and current control, the condition that the DC bus voltage needs to meet is formula (5).

$$V_{DC}^{PV} \geq 2\frac{V_{dq}^{PV}}{D_{dq}} \tag{5}$$

In formula (5), D_{dq} represents the photovoltaic DC voltage modulation coefficient, and V_{dq}^{PV} represents the value of the voltage output by the photovoltaic reverse transformer after dq transformation. The expression for photovoltaic sag control strategy is formula (6).

$$\begin{cases} \omega_{PV} = \omega_n^{PV} - m_P^{PV}\left(P_{PV} - P_{PV}^*\right) + K_{pvdc}^{PV}\left(V_{DC}^{PV} - V_{DC}^{PV\,ref}\right) + K_{ivdc}^{PV}\int\left(V_{DC}^{PV} - V_{DC}^{PV\,ref}\right)dt \\ V_{PV} = V_n^{PV} - n_Q^{PV}\left(Q_{PV} - Q_{PV}^*\right) \end{cases} \tag{6}$$

In formula (6), n_Q^{PV} and m_P^{PV} represent the reactive and active droop coefficients of the PPG system, respectively. V_n^{PV} and ω_n^{PV} respectively represent the rated voltage and

frequency of the PPG system. V_{PV} and ω_{PV} represent the voltage amplitude and output angular frequency of the PPG system, respectively. Q_{PV} and P_{PV} represent the RP and AP output of the photovoltaic inverter, respectively. Q_{PV}^{*} and P_{PV}^{*} represent reference values for the RP and AP output of the photovoltaic inverter.

3.2 A PHMCS combining renewable energy

The state space (SPA) of a system consists of system state variables and input variables. The system input variables have an impact on the external signals of the system, and the system attitude variables are used to describe the dynamic differential equations in the system, which are abstract mathematical variables. When the system experiences imbalance and non-zero input, the state of the system also changes accordingly. The PHMCS's state variables need to be linearised, and the linearisation process starts with selecting the state variables and input variables. The condition that the variable satisfies is formula (7).

$$\dot{x} = f\left(x_0, u_0\right) = 0 \tag{7}$$

In formula (7), x_0 represents the initial state variable and u_0 represents the input vector. After adding a disturbance to the system, formula (8) is obtained.

$$\begin{cases} x = x_0 + \Delta x \\ u = u_0 + \Delta u \end{cases} \tag{8}$$

In formula (8), Δ represents the added disturbance, x represents the selected state variable, and u represents the selected input vector. The expression for the attitude variable after adding disturbance is formula (9).

$$\dot{x} = \dot{x}_0 + \triangle\dot{x} = f\left[\left(x_0 + \Delta x\right), \left(u_0 + \Delta u\right)\right] \tag{9}$$

Formula (9) represents the state variable in the presence of disturbances. After obtaining the perturbation expression formula of the state variable, the nonlinear function is expanded using Taylor technique. Finally, a linearised equation is derived as formula (10).

$$\Delta\dot{x} = A\Delta x + B\Delta u \tag{10}$$

In formula (10), A represents the linearised system matrix, and B represents the coefficients of input variables with perturbations. The A matrix includes parameters such as controllers and circuits, so analysing the A matrix can determine whether the nonlinear system is stable. When there are negative real roots in the eigenvalues of the system characteristic equation, the system tends to be in a stable state. When there is at least one positive real root in the eigenvalues of the system characteristic equation, the system state is unstable. When the eigenvalues have zero real parts, the system stays in a critical stable state. In a wind PG system, the captured wind energy is transmitted by the shaft system to the generator rotor. In a DDWPS, the direct drive generator is synchronised with the speed of the WT, so it can be considered as a whole. The frequency stability of the system is improved by simulating the inertia response of the conventional generator. The relevant motion equation of a permanent magnet WT is expressed as formula (11).

$$J\frac{d\omega_s}{dt} = T_W - T_e \tag{11}$$

In formula (11), J represents the inertia time coefficient of the rotor, and ω_s represents the angular velocity. T_W serves as the mechanical torque of the WT, and T_e serves as the electromagnetic torque of the generator. Drop the mechanical and electromagnetic torque of the WT into the rotor motion equation of the permanent magnet separator, and finally linearise it. The mathematical expression for the intermediate capacitor is formula (12).

$$C_{WT}\frac{dV_{DC}^{WT}}{dt} = \frac{P_g - P_{WT}}{V_{DC}^{WT}} \tag{12}$$

In formula (12), V_{DC}^{WT} represents the voltage of the intermediate DC circuit, and C_{WT} represents the intermediate DC capacitor in the DDWPS.

Figure 4 Circuit diagram of hybrid microgrid (see online version for colours)

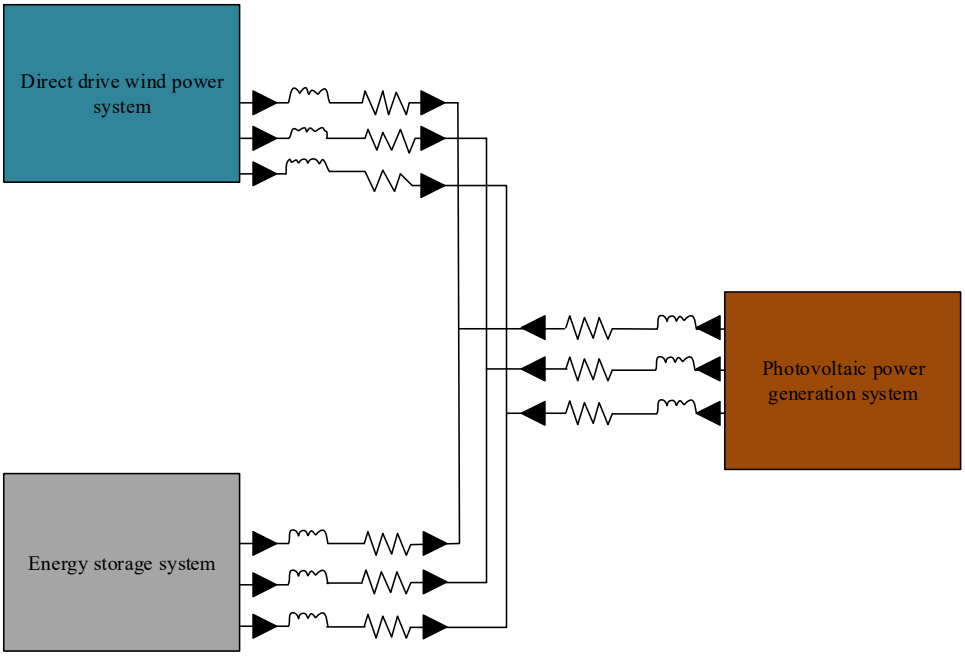

P_{WT} represents the output power of the grid side inverter, and P_g represents the input power of the machine side inverter. The core modules in the PPG system are the photovoltaic array as well as the intermediate DC bus voltage. According to the characteristics, the function relation in the current and voltage of the photovoltaic array is formula (13).

$$i_{PV} = N_p I_{ph} - N_p I_0 \left[\exp\left(\frac{qV_{DC}^{PV}}{KTA_{IF}N_s N_c} \right) - 1 \right] \tag{13}$$

In formula (13), N_p serves as the quantity of parallel series of photovoltaic arrays, and I_{ph} represents the short-circuit current on the photovoltaic panel. I_0 represents reverse

saturation current, N_s serves as the quantity of modules in series, N_c serves as the quantity of photovoltaic cells in series in the photovoltaic module, and A_{IF} represents the ideal factor. The circuit of the hybrid microgrid is shown in Figure 4.

Figure 4 shows the hybrid microgrid. This diagram illustrates the line structure between various parts of a complete hybrid microgrid, including connecting lines, line impedance, and load impedance. The dynamic link of the DC bus in PPG systems can be expressed as formula (14).

$$C_{PV}\frac{dV_{DC}^{PV}}{dt}=i_{PV}-\frac{v_{id}^{PV}i_{Id}^{PV}+v_{iq}^{PV}i_{Iq}^{PV}}{V_{DC}^{PV}} \tag{14}$$

By using formulas (13) and (14), the SPA matrix of the power outer loop of the PPG system could be gotten. By integrating the state models of direct drive wind and PPG, the SPA expression of a PHM combined with new energy can be obtained, as shown in formula (15).

$$\Delta x_{MG}=\left[\Delta x_{WT}\Delta x_{PV}\Delta x_{BESS}\Delta x_{NET}\Delta x_{LOAD}\right]^{T} \tag{15}$$

In formula (15), Δx_{MG} represents the overall spatial state of the PHM, Δx_{NET} serves as the SPA model of the PHM, and Δx_{LOAD} represents the SPA model of the PHM load. Therefore, the PHMCS combined with renewable energy is shown in Figure 5.

Figure 5 Schematic diagram of a control system incorporating renewable energy (see online version for colours)

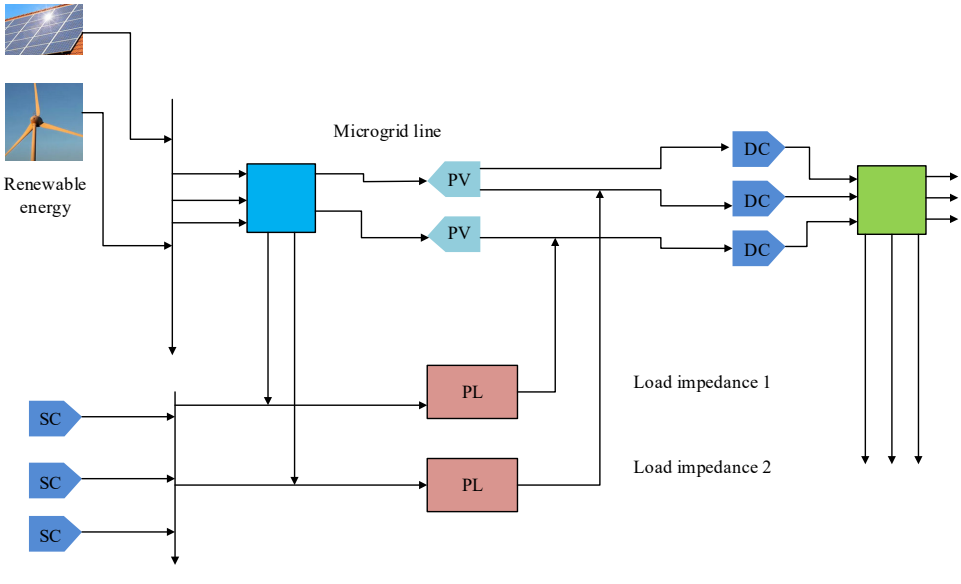

Figure 5 is a schematic diagram of a control system that combines renewable energy. This diagram illustrates the operation process and different modules of the control system.

4 Analysis of PHMCS combined with renewable energy

This study analyses the construction of a PHMCS that combines renewable energy. Firstly, it studies the feasibility of its control strategy, and then explores the stability of PHMs.

4.1 Control strategy of PHM combined with renewable energy

For enhancing the energy utilisation and conversion efficiency of the PHM combined with renewable energy, the maximum power of the system is studied. Wind energy has randomness, instability, and volatility. Therefore, experiments are conducted on WTs at different wind speeds, and the experimental results are shown in Figure 6.

Figure 6 Output power results of WT under different wind speed (see online version for colours)

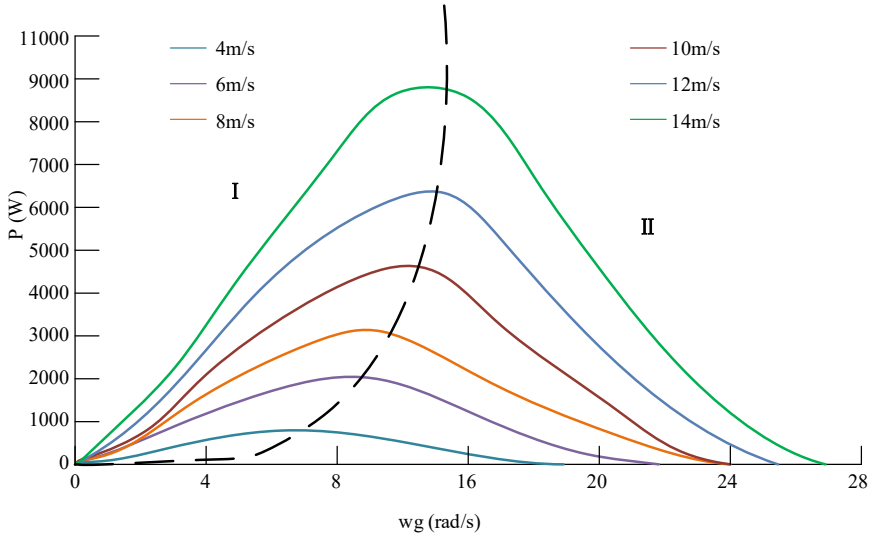

Figure 6 shows the output power results of WTs in various wind speeds. According to the operating mechanism of permanent magnet direct drive WTs, there exists a MPP for direct drive permanent magnet WTs at different wind speeds. This MPP can generate maximum power under different wind speed conditions. The dashed line represents the MPP operating line, and the graph shows that the dashed line divides the wind PG area into two zones I and II. In zone I, the generator speed is below the optimal PG speed, and the output power of the WT increases with the increase of the generator speed. In zone II, the generator speed surpasses the optimal PG speed, and the output power of the WT diminishes as the growth of the generator speed. In zone II, as the load power of the wind PG system increases, the permanent magnet wind motor will diminish its speed and output more power. In zone I, with the load power of the wind PG system increases, the speed of the permanent magnet wind motor continues to rise, which may exceed the operating range and even cause the generator to lose control. Therefore, it operates more stably in zone II and has more ample space to operate permanent magnet generators. In the PPG system, the MPP of the photovoltaic system is tracked, with an ambient

temperature of 25°C and light intensity ranging from 400 W/m^2 to 1,000 W/m^2. The I-V curve and P-V curve results are showed in Figure 7.

Figure 7 I-V and P-V characteristic curves of different light intensities, (a) I-V characteristic curve under different illumination (b) P-V characteristic curve under different illumination (see online version for colours)

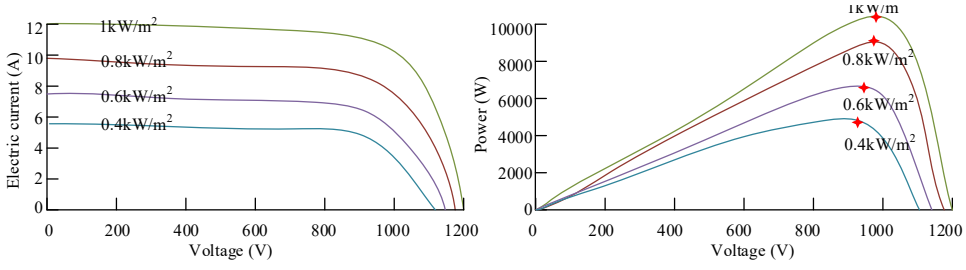

(a) (b)

Figure 7 shows the I-V and P-V characteristic curves for different light intensities. Figure 7(a) shows the I-V curve. The figure shows that as the light intensity increases, the current and voltage also increase, and the amplitude of voltage change is smaller than that of current change. When the light intensity is 800 W/m^2, the current is 10 A and the voltage is 1,160 V, while when the light intensity is 1,000 W/m^2, the current is 12 A and the voltage is 1,200 V. Figure 7(b) depicts the P-V curve, which reveals that each power curve exhibits a MPP. According to the I-V curve, the higher the voltage, the stronger the light intensity, and the higher the voltage, resulting in a higher output power of the photovoltaic array and a higher MPP. Therefore, to achieve higher efficiency in PPG, it is essential for continuously adjusting the light intensity and the MPP of the photovoltaic array, and continuously adjust the control strategy for maintaining the maximum power output of the hybrid microgrid. To verify the proposed PHMC strategy, experiments are conducted on a 30 kVA microgrid system using a distributed DDWPS (PMSG-WT), battery energy storage system (BESS), and PPG system (PV). The experimental results are shown in Figure 8.

Figure 8 shows the dynamic response of a hybrid microgrid under sudden load changes. Figure 8(a) shows the AP waveform of a hybrid microgrid distributed power source. It shows that the VS control strategy of the PPG system is activated at t = 1 s, and the AP gradually stabilises at around 5,000 W after t = 2 s. At t = 1 s, the VS control strategy of the DDWPS is activated, and the AP stabilises at around 6,200 W after t = 6 s. The AP of the battery ES system stabilises at 1,200 W after t = 6 s. Figure 8(b) shows the DC voltage waveforms of a DDWPS and a PPG system. This figure shows that the DC bus voltage gradually stabilises after disturbance in the DDWPS and PPG system after starting the control strategy. It conducts research on the performance of hybrid microgrids under wind speed disturbances, and after t = 6 s, the wind speed is changed from 10 m/s to 9.6 m/s. Experiments are conducted on the above systems. The experimental results are shown in Figure 9.

Figure 8 Dynamic characteristic response of hybrid microgrid under sudden load change, (a) active power waveform of distributed power supply in hybrid microgrid (b) DC voltage waveform of direct drive wind power and photovoltaic power generation system (see online version for colours)

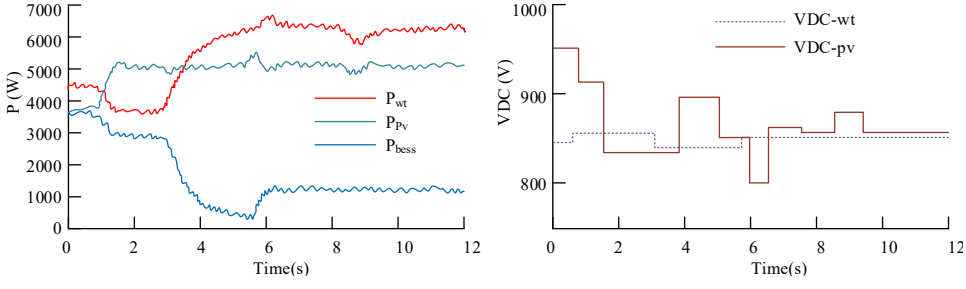

(a) (b)

Figure 9 Dynamic characteristic response of hybrid microgrid when wind speed changes, (a) active power waveform of hybrid microgrid distributed power supply (b) DC voltage waveform of direct drive wind power system and photovoltaic power generation system (c) rotor speed of direct drive permanent magnet generator (see online version for colours)

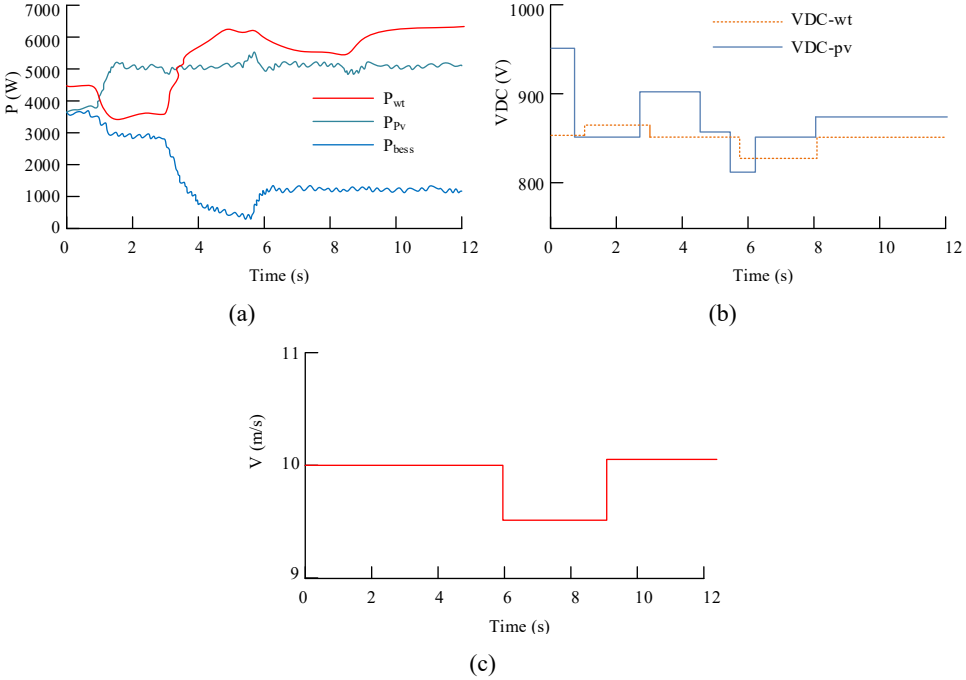

(a) (b)

(c)

Figure 9 shows the dynamic response of a hybrid microgrid under sudden changes in wind speed. Figure 9(a) shows the AP waveform of a hybrid microgrid distributed power source. The figure shows that when t = 6 s, the AP of the PPG system decreases from 6,200 W to 5,500 W. Figure 9(b) shows the DC voltage waveforms of the DDWPS and PPG system. Due to changes in wind speed, the DC bus voltage of the DDWPS reduce from 850 V to 830 V at t = 6 s, and stabilises at 850 V after t = 8 s. Figure 9(c) shows the

rotor speed of a direct drive permanent magnet generator. The speed decreases slightly after $t = 6$ s, and stabilises again at 10 m/s after $t = 9$ s.

4.2 Stability analysis of PHM combined with renewable energy

The study analyses the important participation factors of microgrid systems and explores the performance of hybrid microgrid systems under dominant modes. In a hybrid microgrid, the distribution of dominant mode characteristic values is shown in Figure 10.

Figure 10 Characteristic value distribution of dominant mode of hybrid microgrid (see online version for colours)

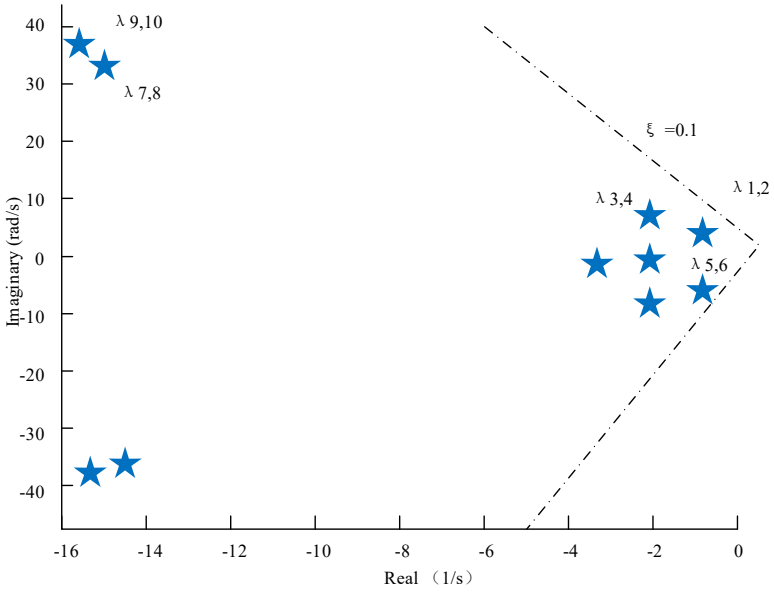

Figure 10 shows the distribution of characteristic values for the dominant mode of hybrid microgrids. The feature roots in the figure are all in the low frequency range. Due to the presence of low-frequency dominant oscillation modes and high-frequency oscillation modes in hybrid microgrid systems, only low-frequency oscillation is studied under small interference conditions. The numerical statistics of characteristic values are showed in Table 2.

Table 2 The characteristic root statistic results of low frequency dominant mode

Eigenvalue numbering	*Numerical value*	*Oscillation frequency*
λ1,2	–0.931 ± 5.946	0.955 Hz
λ3,4	–2.174 ± 9.002	1.357 Hz
λ5,6	–1.956 ± 0.913	0.136 Hz
λ7,8	–15.241 ± 35.849	5.688 Hz
λ9,10	–15.436 ± 36.588	6.742 Hz

Table 2 shows the statistical results of the characteristic roots of low-frequency dominant modes. The data in the table indicates that different characteristic values have different oscillation frequencies, which can analyse the impact of different parts in the hybrid power grid. λ1,2 is related to the DC bus voltage of the DDWPS, while λ3,4 is relevant to the DC bus voltage of the PPG system. λ5,6 is relevant to the generator side DC voltage controller of the DDWPS, while λ7,8,9,10 is relevant to the power droop link of various distributed power sources in the hybrid microgrid. When the DC voltage control coefficient of the photovoltaic wind power system as well as the DDWPS changes, the trajectory of the characteristic values is showed in Figure 11.

Figure 11 The motion path of the eigenvalue after the change of the key coefficient, (a) the movement trajectory change of characteristic value after DC voltage change of photovoltaic power generation system (b) the movement trajectory change of characteristics value after DC voltage change of direct drive wind power system (see online version for colours)

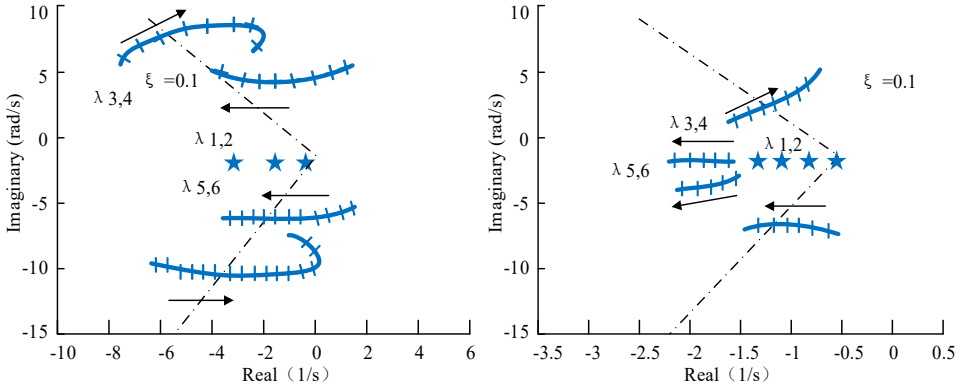

Figure 11 shows the motion trajectory of the eigenvalues after the key coefficient changes. Figure 11(a) shows the trajectory changes of the characteristic values after the DC voltage changes in the PPG system. λ1,2,3,4 move to the left of zero and cross the critical damping line, causing imbalance in the hybrid microgrid. λ7,8 moves towards the right of zero, and the damping ratio gradually weakens. Finally, the DC voltage parameters of the PPG system are optimised to 2e-3. Figure 11(b) shows the trajectory changes of the characteristic values after the DC voltage changes in the DDWPS. The damping ratios of λ1,2,5,6 first decrease and then increase, and do not exceed the critical damping ratio line. λ3,4 moves to the left of zero and cross the zero axis, causing imbalance in the microgrid system. The final DC voltage parameter optimisation for the DDWPS is 1.8e-2. In order to further determine the validity of the research method, the research is tested and compared with recent techniques, as shown in Table 3.

As illustrated in Table 3, the research method exhibits high system stability during operation, with power control accuracy reaching ±0.5% during operation, which is superior to the majority of existing methods. The energy management efficiency of the research method reaches 95%, whereas the energy efficiency of other methods is only 92%. With regard to the issue of extensibility, the research method in question displays considerable potential for extension. From the standpoint of system stability, power control accuracy, energy management efficiency, and scalability, the comprehensive

performance of the research method is optimal. This also demonstrates that the research method is capable of more effective control of PHMs.

Table 3 Test comparison of other methods

Method	*System stability*	*Power control accuracy*	*Energy management efficiency*	*Scalability*	*Test effect*
Research method	High	±0.5%	95%	Strong	Industrial park microgrid, 30% increase in power supply stability
Lv et al. (2020)	Medium	±1.0%	85%	Medium	Urban solar power project, 15% reduction in operational costs
Chang et al. (2022)	Low	±1.5%	80%	Weak	Residential rooftop PV system, 10% increase in self-sufficiency
Tooryan et al. (2022)	Medium	±0.8%	90%	Medium	Remote wind farm, 20% increase in power generation
Hofrichter et al. (2023)	High	±0.3%	92%	Strong	Commercial area energy storage system, 25% optimisation of peak-valley electricity price difference

5 Conclusions

To improve the stability of microgrid control systems and combine renewable energy, a PHMCS is constructed. The study first proposed a DC VS control strategy for direct drive wind and PPG on the ground of their characteristics, and finally established a PHMCS. In a PHM that combines renewable energy, the output power of WTs at various wind speeds was more stable in the right side of the operating line at the MPP. In the I-V and P-V characteristic curves of various light intensities, when the light intensity is 800 W/m^2, the current was 10 A and the voltage was 1,160 V. As the light intensity grows, the current and voltage also increased, and the voltage change amplitude was smaller than the current change amplitude. To maintain the maximum output of the hybrid microgrid, it was necessary to continuously adjust the light intensity and the MPP of the photovoltaic array. In the dynamic response of hybrid microgrids, the VS strategy of PPG systems was activated at t = 1 s. The AP gradually stabilised at around 5,000 W, and the VS control strategy of the DDWPS stabilised at around 6,200 W after t = 6 s. Finally, the effectiveness of the renewable energy PHMCS was verified through considering the important participation factors of the microgrid system. The feasibility of the photovoltaic hybrid micro electric system constructed through research has been verified through experiments. However, there is a persistent low inertia in PPG systems. This can result in the fragility of the entire system. Therefore, virtual inertia can be introduced in subsequent research to continuously improve the system stability of microgrids.

References

Ahmed, R., Nawaz, A., Javid, Z., Khan, M.Y.A., Shah, A.A. and Valarezo, O.M. (2022) 'Optimal transmission switching based on probabilistic load flow in power system with large-scale renewable energy integration', *Electrical Engineering*, Vol. 2, No. 104, pp.883–898.

Azizpour, A., Radmehr, M., Firouzi, M. and Gharehpetian, G.B. (2023) 'Single AC/DC fault current limiter for both side of hybrid AC/DC microgrid', *International Journal of Electronics*, Vol. 110, No. 7, pp.1337–1354.

Badr, M.A.A., Khalil, A.A.I., Khalil, M.M.H., Hafez, A.I. and Mostafa, E.M. (2024) 'Effect of weathering conditions on the durability of solar energy mirrors that heat the HTF oil in El-Kureimat solar energy power plant', *International Journal of Power and Energy Conversion*, Vol. 15, No. 2, pp.99–121.

Chang, J.W., Chae, S. and Lee, G.S. (2022) 'Distributed optimal power sharing strategy in an islanded hybrid AC/DC microgrid to improve efficiency', *IEEE Transactions on Power Delivery*, Vol. 38, No. 1, pp.724–737.

Gupta, P., Kumar, S., Singh, Y.B., Singh, P., Sharm, S.K. and Rathore, N.K. (2022) 'The impact of artificial intelligence on renewable energy systems', *Neuro Quantology*, Vol. 20, No. 16, p.5012.

Hofrichter, A., Rank, D., Heberl, M. and Sterner, M. (2023) 'Determination of the optimal power ratio between electrolysis and renewable energy to investigate the effects on the hydrogen production costs', *International Journal of Hydrogen Energy*, Vol. 48, No. 5, pp.1651–1663.

Kumar, S., Rathore, N.K., Prajapati, M. and Sharma, S.K. (2023a) 'SF-GoeR: an emergency information dissemination routing in flying ad-hoc network to support healthcare monitoring', *Journal of Ambient Intelligence and Humanized Computing*, Vol. 14, No. 7, pp.9343–9353.

Kumar, S., Prajapati, M., Rathore, N.K. and Anand, S.K. (2023b) 'A systematic approach of a flying ad-hoc network for smart cities', *Handbook of Research on Data-Driven Mathematical Modeling in Smart Cities*, pp.55–75, IGI Global, Hershey, Pennsylvania, USA.

Lv, Z., Zhang, Y., Xia, Y. and Wei, W. (2020) 'Adjustable inertia implemented by bidirectional power converter in hybrid AC/DC microgrid', *IET Generation, Transmission & Distribution*, Vol. 14, No. 17, pp.3594–3603.

Mishra, N.K., Mishra, G. and Shukla, M.K. (2024) 'Six-phase DFIG-MPPT synergy: pioneering approaches for maximising energy yield in wind energy generation system', *International Journal of Power and Energy Conversion*, Vol. 15, No. 1, pp.79–98.

Nguyen Duc, T., Tran Thanh, S., Do Van, L., Tran Quoc, N. and Takano, H. (2022) 'Impact of renewable energy integration on a novel method for pricing incentive payments of incentive-based demand response program', *IET Generation, Transmission & Distribution*, Vol. 16, No. 8, pp.1648–1667.

Pande, S., Rathore, N.K. and Purohit, A. (2021) *A Survey and Analysis of Extreme Machine Learning Models and its Techniques*, Tech. Rep. rs-599856/v1, Shri Govindram Seksaria Inst. Technol. Sci., Indore, India.

Pandey, D., Rawat, U., Rathore, N.K., Pandey, K. and Shukla, P.K. (2022) 'Distributed biomedical scheme for controlled recovery of medical encrypted images', *IRBM*, Vol. 43, No. 3, pp.151–160.

Rathore, N.K., Jain, N.K., Shukla, P.K., Rawat, U. and Dubey, R. (2021a) 'Image forgery detection using singular value decomposition with some attacks', *National Academy Science Letters*, Vol. 44, No. 4, pp.331–338.

Rathore, N.K., Pandey, D., Doewes, R.I. and Bhatt, A. (2021b) 'A novel security technique based on controlled pixel based encryption of image blocks for sharing a secret image', *Wireless Personal Communications*, Vol. 121, No. 1, pp.191–207.

Rathore, N.K., Khan, Y., Kumar, S., Singh, P. and Varma, S. (2023) 'An evolutionary algorithmic framework cloud based evidence collection architecture', *Multimedia Tools and Applications*, Vol. 82, No. 26, pp.39867–39895.

Rathore, N.K., Rawat, U. and Kulhari, S.C. (2020) 'Efficient hybrid load balancing algorithm', *National Academy Science Letters*, Vol. 43, No. 2, pp.177–185.

Rathore, R. (2022) 'A study on application of stochastic queuing models for control of congestion and crowding', *International Journal for Global Academic & Scientific Research*, Vol. 1, No. 1, pp.1–7.

Tooryan, F., HassanzadehFard, H., Dargahi, V. and Jin, S. (2022) 'A cost-effective approach for optimal energy management of a hybrid CCHP microgrid with different hydrogen production considering load growth analysis', *International Journal of Hydrogen Energy*, Vol. 47, No. 10, pp.6569–6585.